Neutrino follow-up with the Zwicky Transient Facility: Results from the first 24 campaigns

Robert Stein [1,2,3]⋆, Simeon Reusch [1,2], Anna Franckowiak [1,2,4], Marek Kowalski [1,2],
Jannis Necker [1,2], Sven Weimann [4], Mansi M. Kasliwal [3], Jesper Sollerman [5], Tomas Ahumada [6,7]†,
Pau Amaro Seoane [8,9,10], Shreya Anand [3], Igor Andreoni [11,12,13], Eric C. Bellm [14],
Joshua S. Bloom [15,16], Michael Coughlin [17], Kishalay De [18], Christoffer Fremling [3], Suvi Gezari [19],
Matthew Graham [3], Steven L. Groom [20], George Helou [20], David L. Kaplan [21], Viraj Karambelkar [3],
Albert K.H. Kong [22], Erik C. Kool [5], Massimiliano Lincetto [4], Ashish A. Mahabal [3,23],
Frank J. Masci [20], Michael S. Medford [15,16], Robert Morgan [24], Jakob Nordin [2], Hector Rodriguez [25],
Yashvi Sharma [3], Jakob van Santen [1], Sjoert van Velzen [26], Lin Yan [25]

[1] *Deutsches Elektronen-Synchrotron (DESY), Platanenallee 6, D-15378 Zeuthen, Germany*
[2] *Institut fur Physik, Humboldt-Universität zu Berlin, D-12489 Berlin, Germany*
[3] *Division of Physics, Mathematics, and Astronomy, California Institute of Technology, Pasadena, CA 91125, USA*
[4] *Fakultät für Physik & Astronomie, Ruhr-Universität Bochum, D-44780 Bochum, Germany*
[5] *Oskar Klein Centre, Department of Astronomy, Stockholm University, 10691 Stockholm, Sweden*
[6] *Department of Astronomy, University of Maryland, College Park, MD 20742, USA*
[7] *Astrophysics Science Division, NASA Goddard Space Flight Center, Mail Code 661, Greenbelt, MD 20771, USA*
[8] *Max Planck Institute for Extraterrestrial Physics, Garching, Germany*
[9] *Institute of Applied Mathematics, Academy of Mathematics and Systems Science, CAS, Beijing, China*
[10] *Kavli Institute for Astronomy and Astrophysics, Beijing, China*
[11] *Joint Space-Science Institute, University of Maryland, College Park, MD 20742, USA*
[12] *Department of Astronomy, University of Maryland, College Park, MD 20742, USA*
[13] *Astrophysics Science Division, NASA Goddard Space Flight Center, Mail Code 661, Greenbelt, MD 20771, USA*
[14] *DIRAC Institute, Department of Astronomy, University of Washington, 3910 15th Avenue NE, Seattle, WA 98195, USA*
[15] *Department of Astronomy, University of California, Berkeley, CA 94720-3411, USA*
[16] *Lawrence Berkeley National Laboratory, 1 Cyclotron Road, MS 50B-4206, Berkeley, CA 94720, USA*
[17] *School of Physics and Astronomy, University of Minnesota, Minneapolis, MN 55455, USA*
[18] *MIT-Kavli Institute for Astrophysics and Space Research, 77 Massachusetts Ave., Cambridge, MA 02139, USA*
[19] *Space Telescope Science Institute, 3700 San Martin Dr., Baltimore, MD 21218, USA*
[20] *IPAC, California Institute of Technology, 1200 E. California, CA 91125, USA*
[21] *Center for Gravitation, Cosmology and Astrophysics, Department of Physics, University of Wisconsin-Milwaukee, Milwaukee, WI 53201*
[22] *Institute of Astronomy, National Tsing Hua University, Hsinchu 30013, Taiwan*
[23] *Center for Data Driven Discovery, California Institute of Technology, Pasadena, CA 91125, USA*
[24] *Physics Department, University of Wisconsin-Madison, Madison, WI 53706, USA*
[25] *Caltech Optical Observatories, California Institute of Technology, Pasadena, CA 91125, USA*
[26] *Leiden Observatory, Leiden University, Postbus 9513, 2300 RA, Leiden, The Netherlands*

arXiv:2203.17135v2 [astro-ph.HE] 23 Jun 2022

ABSTRACT

The Zwicky Transient Transient Facility (ZTF) performs a systematic neutrino follow-up program, searching for optical counterparts to high-energy neutrinos with dedicated Target-of-Opportunity (ToO) observations. Since first light in March 2018, ZTF has taken prompt observations for 24 high-quality neutrino alerts from the IceCube Neutrino Observatory, with a median latency of 12.2 hours from initial neutrino detection. From two of these campaigns, we have already reported tidal disruption event (TDE) AT2019dsg and likely TDE AT2019fdr as probable counterparts, suggesting that TDEs contribute >7.8% of the astrophysical neutrino flux. We here present the full results of our program through to December 2021. No additional candidate neutrino sources were identified by our program, allowing us to place the first constraints on the underlying optical luminosity function of astrophysical neutrino sources. Transients with optical absolutes magnitudes brighter that -21 can contribute no more than 87% of the total, while transients brighter than -22 can contribute no more than 58% of the total, neglecting the effect of extinction. These are the the first observational constraints on the neutrino emission of bright populations such as superluminous supernovae. None of the neutrinos were coincident with bright optical AGN flares comparable to that observed for TXS 0506+056/IC170922A, suggesting that most astrophysical neutrinos are not produced during such optical flares. We highlight the outlook for electromagnetic neutrino follow-up programs, including the expected potential for the Rubin Observatory.

Key words: neutrinos – astroparticle physics – transients: tidal disruption events – transients: supernovae – gamma-ray bursts

1 INTRODUCTION

Astrophysical neutrinos are produced through the interaction of accelerated hadrons with matter or photons. A flux of astrophysical neutrinos with energies in the TeV-PeV range, was first discovered by IceCube in 2013 (IceCube Collaboration 2013). Recent results suggest that a substantial fraction of these high-energy neutrinos are produced in the cores of Active Galactic Nuclei (AGN) (Abbasi et al. 2021), with additional evidence for neutrino emission from the nearby AGN NGC 1068 (Aartsen et al. 2020). Beyond this static component, various transient or variable source classes have been proposed as possible contributors to the neutrino flux, including gamma-ray bursts (GRBs) (Waxman & Bahcall 1997), core-collapse supernovae (CCSNe) (Murase et al. 2011), TDEs (Farrar & Gruzinov 2009) and blazars (Mannheim 1993). All of these proposed neutrino source classes have electromagnetic signatures at optical wavelengths.

To aid in identifying these time-varying source candidates, IceCube has operated an automated program since 2016 to publish realtime high-energy neutrino alerts (Aartsen et al. 2017), enabling contemporaneous electromagnetic observations of putative neutrino source candidates at radio (Kadler et al. 2021), optical (Kowalski & Mohr 2007; Aartsen et al. 2015; Pan-Starrs Collaboration et al. 2019; Morgan et al. 2019, Necker et al. in prep), X-ray (Evans et al. 2015; Ferrigno et al. 2021), and gamma-ray wavelengths (Lucarelli et al. 2019; Garrappa et al. 2021; Satalecka et al. 2021). In 2017, this realtime program led to the identification of a flaring blazar, TXS 0506+056, as the likely source of high-energy neutrino IC170922A (IceCube Collaboration et al. 2018). Studies of these high-energy neutrino alerts have suggested possible correlations with blazar sub-populations, namely radio-bright blazars (Plavin et al. 2020, 2021) and intermediate-energy/high-energy peaked blazars (IBLs/HBLs) (Giommi et al. 2020a).

The Zwicky Transient Facility (ZTF) is an optical telescope with a 47 sq. deg field of view (Bellm et al. 2019a; Dekany et al. 2020). Since first light in 2018, ZTF has operated a dedicated neutrino follow-up program, in which the arrival directions of IceCube neutrino alerts are observed with Target-of-Opportunity (ToO) observations (Graham et al. 2019). This program has led to the identification of two further likely high-energy neutrino sources, the TDE AT2019dsg (Stein et al. 2021b) and the probable TDE AT2019fdr (Reusch et al. 2021a). Accounting for the contribution of higher-redshift sources, these results suggest that at least 7.8% of neutrino alerts arise from the broader TDE population (Reusch et al. 2021a). Archival analysis of ZTF data revealed further evidence of a correlation between such flares and high-energy neutrinos (van Velzen et al. 2021).

In this paper we outline the full results of the ZTF neutrino follow-up program, which has to date included 24 dedicated neutrino follow-up campaigns. This sample enables novel constraints to be set on the neutrino emission of a broad range of optical transient and variable populations.

The paper is organised as follows: Section 2 outlines the program itself, including trigger criteria and optical candidate selection. Section 3 outlines transient candidates identified by the program, and subsequent electromagnetic observations to determine their nature. Section 4 outlines optical AGN flares found coincident with neutrinos, and Section 5 provides data on two candidate neutrino sources identified in the literature. Section 6 considers the various constraints that can be placed on different possible neutrino source populations from our program. Section 7 summarises the main results, and outlines how such follow-up programs may improve with future observatories.

2 NEUTRINO FOLLOW-UP WITH ZTF

Neutrino alerts are generally published by IceCube in the form of automated Gamma-ray Coordination Network (GCN) Notices[1], with initial estimates of the statistical uncertainty on the neutrino position. These positions are then superseded after a few hours by a GCN Circular with an updated localisation that also incorporates systematic uncertainties (Lagunas Gualda et al. 2021). Given the substantial increase in localisation area once systematic effects are accounted for,

---

⋆ E-mail: rdstein@caltech.edu
† LSSTC Data Science Fellow
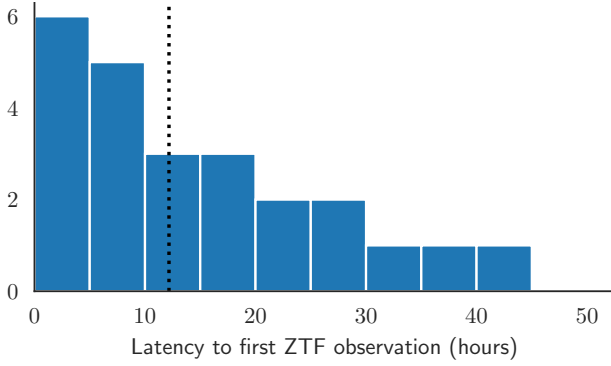
---

[1] https://gcn.gsfc.nasa.gov

Figure 1. Latency between neutrino detection and first ZTF coverage. The median latency time of 12.2 hours is indicated by the vertical dotted line.

with increases of factor 5 not being uncommon, we rely on the latter category to perform our search for neutrino counterparts.

With ZTF, we aim to observe all accessible high-quality neutrino alerts from IceCube. We define high-quality alerts as those with a high probability to be of astrophysical origin ('signalness' > 50%), or those which are well-localised (a 90% localisation area < 10 sq. deg.). Though IceCube labels alerts as Gold or Bronze based on average quality, individual Bronze alerts have been reported with signalness values greater than 50% (e.g. IC211208A) and Gold alerts have been reported with signalness values less than 15% (e.g. IC201130A). We therefore ignore the labelling of these streams, and select exclusively based on the signalness and localisation.

We have followed up 24 neutrinos in the period from survey start on 2018 March 20 to 2021 December 31, out of a total of 79 neutrino alerts published by IceCube during that time. Table 1 summarises each neutrino alert observed by ZTF. From 2019 June 17, IceCube published neutrino alerts with improved selection criteria (V2) to provide an elevated alert rate (Blaufuss et al. 2019). In addition to 1 of the 12 alerts under the old selection, ZTF followed up 23 of the 67 alerts published under the V2 selection. Midway through the ZTF program, an additional cut on neutrino alert galactic latitude ($|b| > 10$ deg) was introduced to avoid crowded fields with many stars.

Each neutrino localisation region can typically be covered by one or two observations of fields in a predefined ZTF 'grid' tiling of the sky. Multiple observations are scheduled for each field, with both g and r filters, and a separation of at least 15 minutes between images. These observations typically last for 300 s, with a typical limiting magnitude of 21.5. ToO observations are typically conducted on the first two nights following a neutrino alert, before swapping to serendipitous coverage with shorter 30 s exposures and a 2-day cadence as part of the public survey (Bellm et al. 2019b). As can be seen in Figure 1, our first coverage of events has a median latency of 12.2 hours from neutrino detection. Some latency is unavoidable because the neutrino localisation itself is typically only released with a delay of $\gtrsim 2$ hours, but additional latency arises primarily due to observability constraints. Poor weather can prevent observations on the first night after neutrino detection, leading to 20% of alerts observed with a latency >24 hours. Serendipitous coverage from the public survey, with a median latency of 24 hours after neutrino detection, reduces the latency for some campaigns.

As for all ZTF data, these observations are first processed by the Infra-red Processing and Analysis Centre (IPAC) to identify detections in difference images (Masci et al. 2019). These detections are then packaged as 'alerts' (Patterson et al. 2019), and processed by our dedicated data analysis pipeline, *NuZTF* (Stein et al. 2021a),

which searches for extragalactic ZTF detections coincident with external triggers. For neutrinos followed-up by ZTF, we define spatial coincidence as requiring that an object lies within the reported 90% localisation rectangle from IceCube, and define temporal coincidence as requiring that an object is detected at least once following the neutrino arrival time.

NuZTF is built using the *AMPEL* software framework (Nordin et al. 2019), based on a search algorithm for extragalactic transients. Cuts are applied to reject spurious detections, stars and solar system objects (see Stein et al. 2021b for more details). Searching for detections in the window from neutrino arrival time to 14 days post-neutrino, these cuts typically yield 1 good candidate per ~3 sq. deg. of observed sky.

Promising candidates are prioritised for spectroscopic classification, to confirm or rule out a possible association with a given neutrino. Once classified, an object can then be cross-referenced to relevant neutrino emission scenarios for that population. In particular, optical signatures we look for include:

- **Supernovae with evidence of CSM interaction**. High-energy neutrinos are thought to be produced when CCSNe occur within a dense circumstellar medium (CSM), with the resultant shock collisions then generating neutrino emission (Murase et al. 2011). The presence of such CSM interaction also results in characteristic narrow lines in the optical spectrum, so these models generally apply to the Type IIn supernova population which exhibits these lines. The neutrino emission is expected to be highest close to optical peak, and to then decay over time. In this case, the expected optical signature would be any supernova with evidence of ongoing CSM interaction.

- **Supernovae with relativistic jets**. Some supernovae have been observed to launch relativistic jets as part of the core-collapse process (Galama et al. 1998). Those jets which proceed to escape the surrounding stellar envelope and CSM can be observed as long GRBs if they are oriented towards Earth. Analogously, where an on-axis supernova jet does not escape the stellar envelope, there would instead be a so-called 'choked jet' (Nakar 2015). For both scenarios, neutrino emission would primarily be expected during the 'prompt phase', in the ~100s after supernova explosion (Waxman & Bahcall 1997; Senno et al. 2016). This scenario would then lead to a young supernova, typically of Type Ic-BL, appearing at the location of the neutrino. The supernova would have an explosion time compatible with the neutrino detection time, and since SNe brighten over a period of days, this optical signature would be delayed relative to the neutrino itself.

- **GRB Afterglows.** Another signature of the supernova jet scenario would be the direct detection of a long-GRB afterglow. Models have also predicted neutrino emission for short GRBs, so a short-GRB afterglow could also be a potential counterpart (Waxman & Bahcall 1997). These GRB afterglows would not be detected before the neutrino detection, and would fade rapidly over the next few hours before falling below the ZTF detection threshold.

- **AGN Flares**. AGN flares, and especially blazar flares, have been suggested as neutrino sources (Bednarek & Protheroe 1999), though the neutrino emission itself would not necessarily be directly correlated to the optical emission. For example, for the standard two-hump Spectral Energy Distribution (SED) model, the optical emission could serve primarily as a tracer for photon target density but not necessarily PeV proton luminosity. We restrict ourselves to searches for AGN undergoing significant optical flaring coincident

Event	R.A. (J2000) [deg]	Dec (J2000) [deg]	90% area [sq. deg.]	ZTF obs [sq. deg.]	Latency [hours]	Signalness	References
IC190503A	120.28	+6.35	1.9	1.4	10.2	36%	Blaufuss (2019c) Stein et al. (2019a)
IC190619A	343.26	+10.73	27.2	21.6	20.9	55%	Blaufuss (2019e) Stein et al. (2019b)
IC190730A	225.79	+10.47	5.4	4.5	7.5	67%	Stein (2019a) Stein et al. (2019c)
IC190922B	5.76	−1.57	4.5	4.1	8.0	51%	Blaufuss (2019h) Stein et al. (2019d)
IC191001A	314.08	+12.94	25.5	23.1	7.4	59%	Stein (2019c) Stein et al. (2019e)
IC200107A	148.18	+35.46	7.6	6.3	2.0	–	Stein (2020a) Stein & Reusch (2020)
IC200109A	164.49	+11.87	22.5	22.4	32.4	77%	Stein (2020b) Reusch & Stein (2020a)
IC200117A	116.24	+29.14	2.9	2.7	22.0	38%	Lagunas Gualda (2020a) Reusch & Stein (2020b) Reusch & Stein (2020c)
IC200512A	295.18	+15.79	9.8	9.3	1.7	32%	Lagunas Gualda (2020c) Reusch et al. (2020a)
IC200530A	255.37	+26.61	25.3	22.0	0.2	59%	Stein (2020e) Reusch et al. (2020b) Reusch et al. (2020c)
IC200620A	162.11	+11.95	1.7	1.2	25.8	32%	Santander (2020b) Reusch et al. (2020e)
IC200916A	109.78	+14.36	4.2	3.6	14.7	32%	Blaufuss (2020e) Reusch et al. (2020f) Reusch et al. (2020g)
IC200926A	96.46	−4.33	1.7	1.3	4.1	44%	Lagunas Gualda (2020g) Reusch et al. (2020h)
IC200929A	29.53	+3.47	1.1	0.9	14.1	47%	Lagunas Gualda (2020h) Weimann et al. (2020a)
IC201007A	265.17	+5.34	0.6	0.6	4.8	88%	Santander (2020c) Reusch et al. (2020i)
IC201021A	260.82	+14.55	6.9	6.3	43.7	30%	Lagunas Gualda (2020i) Stein et al. (2020b)
IC201130A	30.54	−12.10	5.4	4.5	7.1	15%	Lagunas Gualda (2020l) Weimann et al. (2020b)
IC201209A	6.86	−9.25	4.7	3.2	16.9	19%	Lagunas Gualda (2020m) Reusch et al. (2020j)
IC201222A	206.37	+13.44	1.5	1.4	35.2	53%	Blaufuss (2020k) Stein et al. (2020c)
IC210210A	206.06	+4.78	2.8	2.1	0.2	65%	Lagunas Gualda (2021a) Reusch et al. (2021b)
IC210510A	268.42	+3.81	4.0	3.7	5.1	28%	Santander (2021c) Stein et al. (2021c)
IC210629A	340.75	+12.94	6.0	4.6	15.4	35%	Santander (2021f) Necker et al. (2021)
IC210811A	270.79	+25.28	3.2	2.7	26.7	66%	Santander (2021h) Stein et al. (2021d)
IC210922A	60.73	−4.18	1.6	1.2	16.1	92%	Lincetto (2021a) Weimann et al. (2021)

Table 1. Summary of the 24 neutrino alerts followed up by ZTF since survey start on 2018 March 20.

with a neutrino. Neutrinos could also be produced in AGN without coincident optical flares, but such neutrino emission scenarios are not best probed with an optical follow-up program such as ours.

• **Tidal Disruption Events**. TDEs have been suggested as neutrino sources, through multiple emission channels such as jets, outflows or in coronae (see Hayasaki 2021 for a recent review). The timescale for neutrino production remains unclear, but would not be expected prior to the TDE itself. Non-thermal emission from TDEs can last several hundred days, so the signature in this case would be any 'ongoing' TDE coincident with a neutrino.

We do not explicitly reject objects with a history of variability, because variable objects have been proposed as possible neutrino sources. However, our program is intended to identify increased optical flux that is contemporaneous with a neutrino's detection, so only variable objects with significantly enhanced flux relative to reference images are selected by our pipeline. The blazar flare of TXS 0506+056 fell into this category (IceCube Collaboration et al. 2018), and we would be capable of identifying similar examples.

To date, the *NuZTF* pipeline has identified 172 candidates for visual inspection out of an observed area of 154.33 sq. deg across 24 neutrinos, using a search window of 14 days after each neutrino detection. This corresponds to an initial density of 1.05 candidates per sq. deg. of sky. The full list of candidates for each neutrino is given in the Appendix.

Visual inspection then enables us to further classify objects and reject background detections. Viewing difference images directly enables us to identify additional image artefacts. We select likely stars through cross-matches to Gaia (Gaia Collaboration et al. 2018), where we reject sources with significant (3σ) evidence for parallax, and to SDSS star/galaxy morphology classifications (Stoughton et al. 2002).

We then flag AGN through matches to catalogued sources in the Milliquas catalogue (Flesch 2021), or via WISE colour cuts (Wright et al. 2010; Stern et al. 2012). We seek to distinguish between 'routine' AGN variability and extreme AGN flares. We search for evidence of flaring activity at the time of neutrino detection using the data provided in the ZTF alert packets (Patterson et al. 2019), which are based on difference images. For cases where a source appears to be significantly variable, or may have been flaring at the time of neutrino detection, we run dedicated forced photometry on the science images to produce a source lightcurve (Masci et al. 2019). We reject AGN with no evidence for contemporaneous flaring as 'AGN variability'. After removing those sources flagged as stars (17), image artefacts (17) or AGN variability (84), we are left with 54 'interesting candidates'. The full breakdown in classification is shown in Figure 2.

These interesting candidates include potential transients, which we seek to classify spectroscopically. Some objects will have already been classified serendipitously, in particular those brighter than 19.0 mag selected by the ZTF Bright Transient Survey (Fremling et al. 2020; Perley et al. 2020). The efficiency with which candidates were classified can be seen in Figure 3. Above a peak apparent magnitude of 19.5, almost all candidates are classified. There were 106 fainter candidates in total, of which 68% were classified. The spectroscopic programs which supported our program are listed in Table 2.

The transients are further broken down by subclass in Figure 4. Four could be immediately excluded as candidates based on their classification as SNe Ia, a population not predicted to emit neutrinos. Of the remainder, beyond the two TDEs, no further sources exhib-
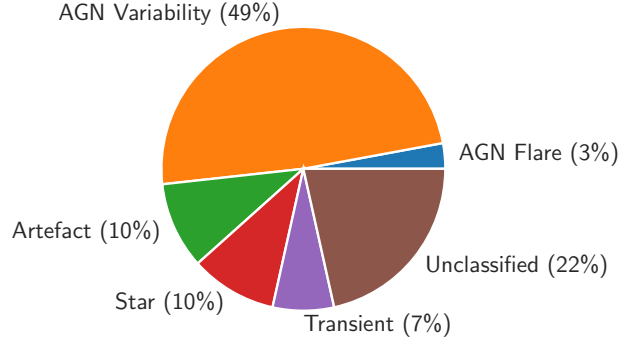
Figure 2. Breakdown of the classification of 172 candidates selected by our program for visual inspection.
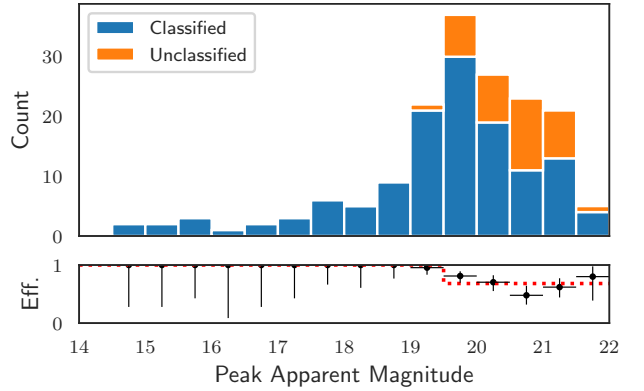
Figure 3. Top: Apparent magnitude distribution of candidates selected for visual inspection. Bottom: Classification efficiency as a function of peak apparent magnitude. The red dashed line indicates our step-function approximation of classification efficiency.

Instrument	Programs
SEDm	2018, 2019, 2020, 2021
NOT	2021B (OPT21B_50, PI: Franckowiak)
	2021B (P64-112)
	2021B (P61-501)
	2022A (22A013, PI: Franckowiak)
TNG	2021B (OPT21B_50, PI: Franckowiak)
	2022A (22A01, PI: Franckowiak)
GEMINI	2021A (GN-2021A-Q-116, PI: Kasliwal)
	2021B (GN-2021B-Q-117, PI: Kasliwal)
GTC	2020B (GTC73-20B, PI: Amaro Seoane)

Table 2. Summary of dedicated spectroscopic programs for our neutrino follow-up program.

ited electromagnetic signatures consistent with the neutrino emission scenarios listed above.

A selection of highlighted results is given in the following sections. ZTF data for three other candidate neutrino sources from the literature, PKS 1502+106, BZB J0955+3551 and PKS 0735+178 are also outlined in Section 5. We omit ZTF data for the probable neutrino-TDEs AT2019dsg and AT2019fdr, as these have already been released in dedicated publications (Stein et al. 2021b; Reusch et al. 2021a).
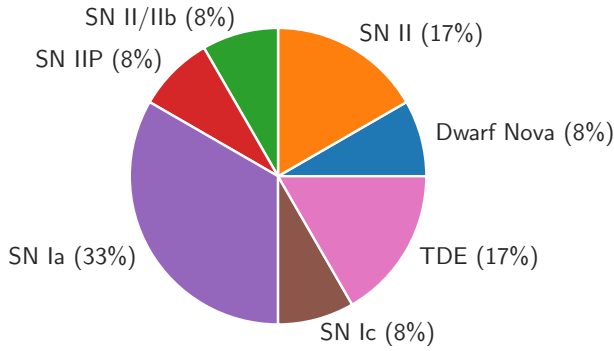
Figure 4. Breakdown of the 12 identified transients by subclass.
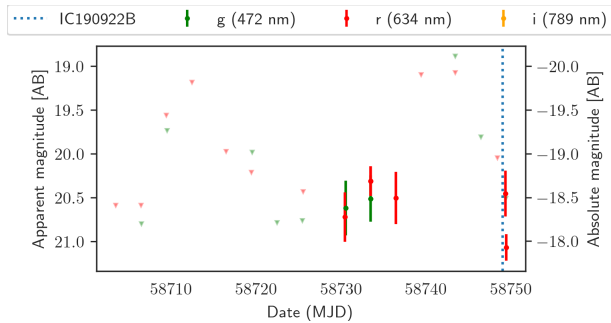
Figure 5. ZTF lightcurve of SN 2019pqh. The arrival time of neutrino IC190922B is marked by the dashed blue line.

3 CANDIDATE TRANSIENT COUNTERPARTS

3.1 SN 2019pqh and IC190922B

Follow-up of IC190922B by ZTF identified the candidate supernova SN 2019pqh/ZTF19abxtupj (Stein et al. 2019d). The lightcurve is shown in Figure 5, where upper limits are illustrated with triangles. The arrival time of the neutrino on 2019 September 22 is marked with a dotted line, and the supernova is detected in the subsequent ToO observations. The neutrino arrival time was close to optical peak, consistent with a CSM-interaction scenario.

However, a spectrum was taken by the *NUTS2 collaboration* (Holmbo et al. 2019), and the supernova was classified as a Type II supernova without spectroscopic signatures of CSM interaction (Reguitti et al. 2019). A higher-resolution spectrum of the object was also obtained on 2019 September 28, shown in Figure 6, using the *Low Resolution Imaging Spectrometer* (LRIS) spectrograph at the Keck observatory (PI: Yan) (Oke et al. 1995). A historical spectrum of the host galaxy, taken by the *Sloan Digital Sky Survey* (SDSS; Abolfathi et al. (2018)), is also shown in Figure 6. Both the transient and host galaxy exhibit prominent Balmer lines, highlighted in orange in Figure 6, from which a redshift of 0.134 is derived. A template-matching classification using SNID (Blondin & Tonry 2007) confirms a Type II supernova classification, with the best match being a Type IIb supernova (SN 1993J, Barbon et al. 1995) 2 days before peak, also shown in Figure 6.

With this redshift, a peak absolute magnitude of -18.6 was derived, atypically bright for such a Type II supernova (see e.g. Lyman et al. 2016). One explanation for this enhanced luminosity could be CSM interaction, through which additional kinetic energy is converted to electromagnetic emission. However, the lack of corresponding narrow line spectroscopic signatures generally disfavours the existence of CSM-interaction, and thus any associated neutrino
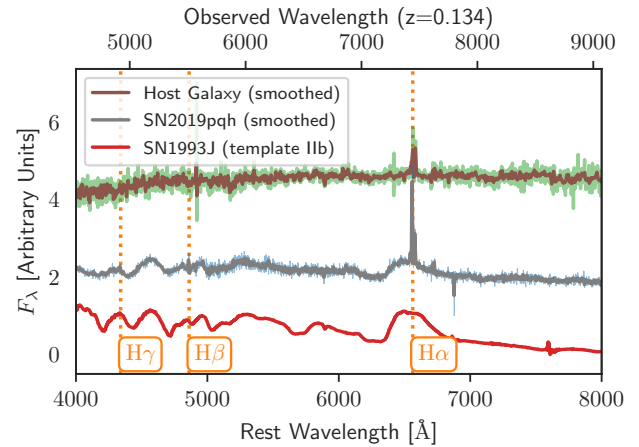
Figure 6. Spectrum of SN2019pqh, taken on 2019 September 28. A historical spectrum of the host galaxy taken by SDSS, and a similar spectrum of a Type IIb supernova, are provided for comparison.

emission from this object. It is therefore likely that SN 2019pqh is instead unrelated to the neutrino IC190922B.

3.2 SN 2020lam and IC200530A

ZTF serendipitously observed the localisation of neutrino alert IC200530A on 2020 May 30, just 10 minutes after detection (Stein 2020e), as part of routine survey operations (Reusch et al. 2020b). Additional ToO observations were then conducted on 2020 May 31 in *g* and *r* band, and again on 2020 June 1. During ZTF follow-up of IC200530A, SN 2020lam/ZTF20abbpkpa was identified as a candidate supernova and potential optical counterpart (Reusch et al. 2020b). Spectroscopic observations were triggered using the NOT/ALFOSC spectrograph on 2020 June 6 (PI: Sollerman), which confirmed SN2020lam as a Type II supernova (Reusch et al. 2020c) using SNID. This spectrum is shown in Figure 7, alongside the matching Type IIP supernova (SN 2005cs, Pastorello et al. 2006) mapped to the same redshift.

As seen in the lightcurve in Figure 8, the supernova was close to peak at neutrino detection time. The object then rapidly cooled, and thus reddened, as is typical for supernovae. Given the neutrino arrival time, CSM-interaction would be the only viable neutrino production mechanism. However, the spectrum shown in Figure 7 had no narrow lines, and therefore did not provide any evidence supporting such CSM interaction. SN 2020lam was therefore likely unrelated to IC200530A.

3.3 SN 2020lls and IC200530A

SN 2020lls/ZTF20abdnpdo was also identified as a candidate supernova on 2020 May 30, during ZTF follow-up of IC200530A (Reusch et al. 2020b). Spectroscopic observations were again triggered using the NOT/ALFOSC spectrograph on 2020 June 12 (PI: Sollerman), which confirmed that SN 2020lls was a Type Ic supernova without broad-line features (Reusch et al. 2020d). This spectrum is illustrated in Figure 9, alongside a matching Type Ic supernova spectrum from SNID mapped to the same redshift (Taubenberger et al. 2006). Given that the supernova had not been detected in alert data prior to the neutrino arrival time, and that it belonged to the subpopulation associated with relativistic jets, SN 2020lls was a candidate for the choked-jet neutrino production model.

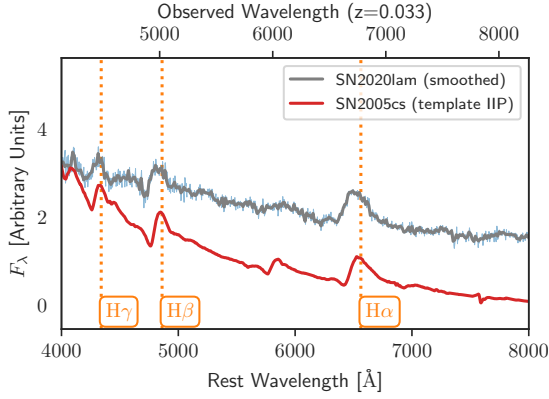**Figure 7.** Spectrum of SN2020lam, taken on 2020 June 6. A similar spectrum, from Type IIP supernova SN 2005cs, is shown for comparison.
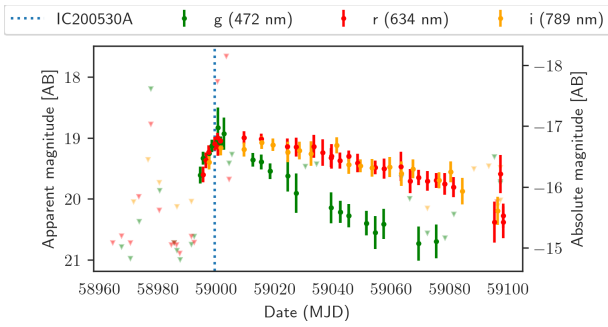

Figure 8. ZTF lightcurve of SN2020lam. The arrival time of neutrino IC200530A is marked by the dashed blue line.
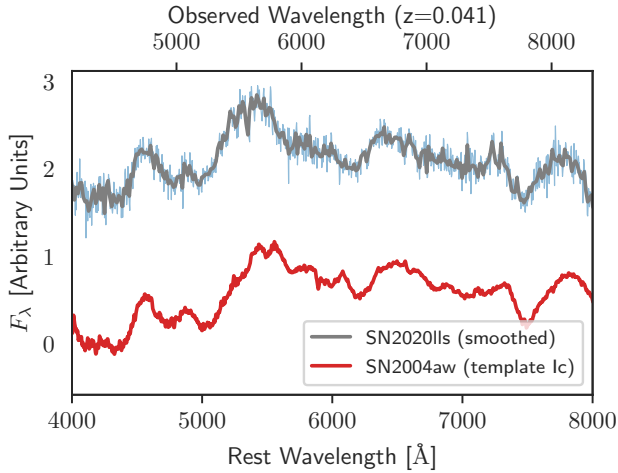

Figure 9. Spectrum of SN 2019lls, taken on 2020 June 13. A similar spectrum, of Type Ic supernova SN 2004aw, is shown for comparison.

However, as can be seen in Figure 10, forced photometry analysis (Reusch 2020) revealed a lower-threshold *i*-band ZTF detection preceding the neutrino arrival. Additionally, modelling of the lightcurve using the *MOSFIT* software (Guillochon et al. 2018) revealed an estimated explosion date predating the neutrino by a week. In combination, these results disfavoured any supernova explosion origin for the neutrino, suggesting that SN 2020lls was instead unrelated to IC200530A (Reusch et al. 2020d).
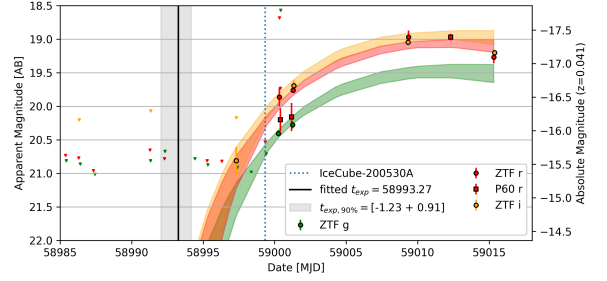

Figure 10. ZTF lightcurve of SN2020lls. The arrival time of neutrino IC200530A is marked with the blue dotted line. The supernova model fit from *MOSFIT* is indicated by the shaded orange/red/green bands, and the the best-fit explosion time is given by the vertical black line.

4 AGN FLARE CANDIDATES

While the vast majority of AGN detections from our pipeline were categorised as 'AGN variability', visual inspection revealed five AGN which appeared to possibly undergo optical flaring at the time of neutrino detection. The forced photometry lightcurves of these five flares are shown in Figure 11. We attempt to quantify whether the optical lightcurves of these AGN identify them as candidate neutrino sources.

We can consider possible optical signatures associated with neutrino emission. One scenario is the optical flaring observed for TXS 0506+056 during the detection of neutrino IC170922A (IceCube Collaboration et al. 2018). In particular, the optical apparent V-band magnitude of TXS 0506+056 was observed to increase from 15.0 to 14.5 during the time of neutrino detection, corresponding to a flux increase of >50%, over a period of 50 days, relative to the pre-neutrino baseline.

AGN can also exhibit short-term variability for periods of hours or days, but we caution that the detection of a high-energy neutrino alert is a process that requires a substantial fluence at the IceCube detector, even after accounting for the significant Eddington bias associated with cosmic neutrino detection (Strotjohann et al. 2019). The corresponding neutrino flux that is required is inversely proportional to the duration of neutrino emission, and therefore associating a neutrino detection with a temporary electromagnetic signature lasting hours or days would imply an extremely high average neutrino flux for the duration of that signature. Such highly luminous rapid neutrino flares are not well motivated theoretically, it is therefore unlikely that short AGN flares are indicators of neutrino production.

In contrast, longer-term electromagnetic signatures can serve as tracers for neutrino emission. For example, month-long flaring periods of substantially elevated flux can dominate the neutrino emission of blazars (see e.g. Rodrigues et al. 2021). Very long flares, with durations of years, could also be relevant for neutrino production. However, given the relatively short baseline of ZTF observations, our neutrino follow-up program is not well-suited to identify them. We therefore restrict ourselves to searching for such month-long optical flares, as was observed for TXS 0506+056.

We calculate the median flux for each of the five AGN, and each ZTF filter, in a ±25 day window centered on the neutrino detection. We divide this instantaneous flux by the median flux of the source in that filter over the entire ~4 year ZTF baseline, giving a proxy for relative optical flare strength. These values are given in Table 3. Of the five AGN, only two (ZTF18aavecmo and ZTF20aamoxyt) had a median instantaneous flux >50% above the baseline median flux. ZTF18aavecmo reached this threshold in both g and r band,

while ZTF20aamoxyt reached this threshold only in r. We conclude that the remaining three AGN (ZTF18abrwqpr, ZTF18abxrpgu, ZTF19aasfvqm) do not exhibit substantial neutrino-coincident optical flares, and we therefore find no evidence to suggest they are counterparts to high-energy neutrinos.

ZTF18aavecmo (top panel of Figure 11), cross-matched to source WISEA J170539.32+273641.2, is classified as a likely QSO in the Milliquas catalogue. It underwent a single coherent flare lasting approximately one year, with a peak flux roughly triple the quiescent flux measured by ZTF. It was coincident with neutrino IC200530A, detected during the decay of the optical flare. However, this flare was extremely faint, with a median flux at the time of neutrino detection was $\nu F_\nu \approx 5 \times 10^{-13}$ erg cm^{-2} s^{-1}. This is a factor of 20 lower than the flux observed for TXS 0506+056 during the detection of IC170922A (IceCube Collaboration et al. 2018).

ZTF20aamoxyt (middle panel of Figure 11) is a likely AGN flare, detected coincident with IC200929A. It appears to be spatially consistent with its host galaxy nucleus, and cross-matched to WISEA J015853.53+035126.6. Based on a WISE colour of W1−W2=0.7, it is a possible AGN. The neutrino IC200929A was detected during an extended year-long flare. Much like ZTF18aavecmo, ZTF20aamoxyt at the time of neutrino detection was substantially fainter than TXS 0506+056, with a median flux of $\nu F_\nu \approx 3 \times 10^{-13}$ erg cm^{-2} s^{-1}.

We thus identify no optical AGN flares which resemble the multi-wavelength flare of TXS 0506+056 in 2017, from any of our 24 neutrino follow-up campaigns. While our results do not preclude a significant degree of neutrino emission from AGN more broadly, they disfavour scenarios where the vast majority of astrophysical neutrinos are produced by bright AGN optical flares. There is no tension with scenarios where AGN neutrino emission is not dominated by bright optical flares, for example the 'steady state' AGN neutrino models tested in Abbasi et al. (2021) or scenarios where AGN neutrino emission is correlated only to gamma-ray flares. A more systematic study of correlations between ZTF-detected AGN flares and neutrinos, including calculations of chance coincidence probabilities, will be the subject of a future analysis.

5 CANDIDATE NEUTRINO SOURCES FROM THE LITERATURE

We here provide data on two candidate neutrino sources reported in the literature. However, we caution that none of the objects presented here were selected by our pipeline as ZTF candidates, and therefore are not considered part of our systematic search for neutrino counterparts. We would not claim any such object as a candidate neutrino sources in our neutrino follow-up program, because the chance coincidence probability would be unquantifiable. Any search for additional candidate neutrino sources, beyond those candidates found by our pipeline following ToO observations, would require an independent and unbiased systematic analysis procedure.

5.1 PKS 1502+106

The neutrino IC190730A was reported by IceCube in spatial coincidence with PKS 1502+106 (Stein 2019a), a particularly gamma-bright Flat Spectrum Radio Quasar (FSRQ) with a catalogued redshift of z=1.84 (Albareti et al. 2017) . The object was observed by ZTF as part of ToO observations, and was detected under the ZTF candidate name ZTF18aaqnqzx (Stein et al. 2019c). The blazar had already been repeatedly detected as part of the routine survey opera-
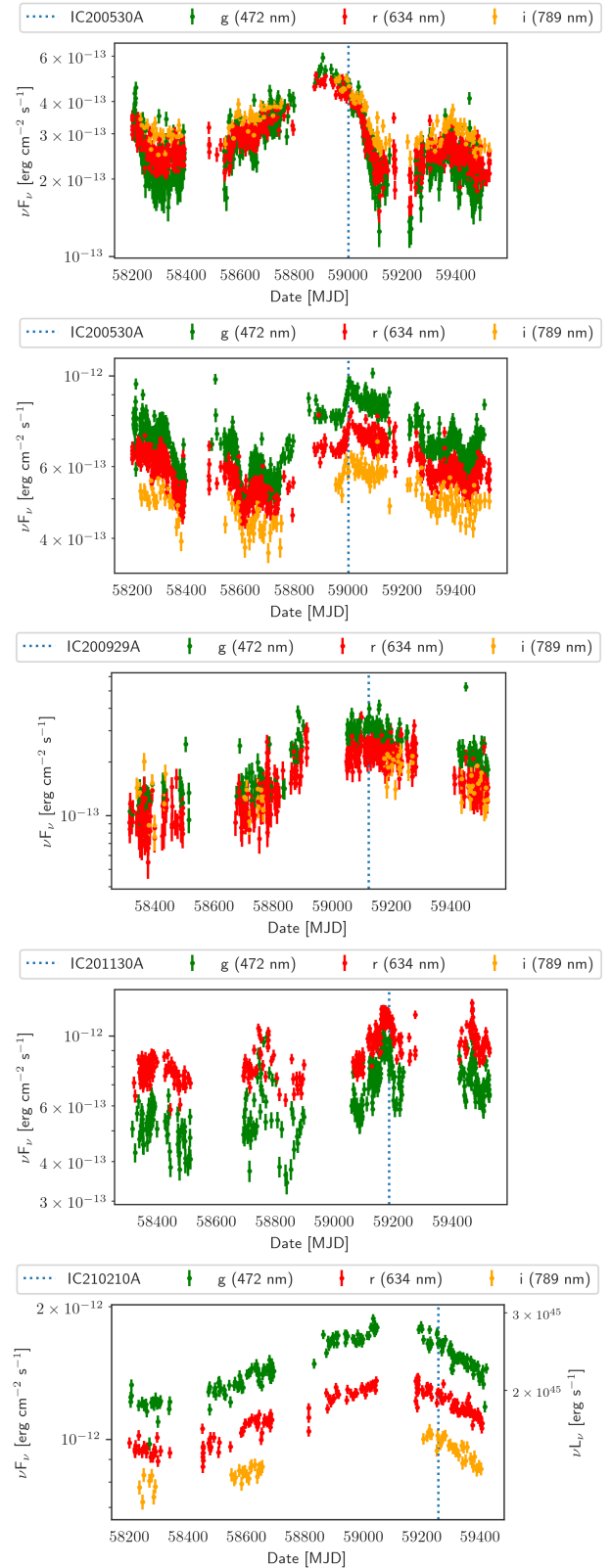

Figure 11. ZTF lightcurve of 5 AGN flares coincident with high-energy neutrinos. From top to bottom, the sources are: ZTF18aavecmo, ZTF18abrwqpr, ZTF20aamoxyt, ZTF18abxrpgu, ZTF19aasfvqm.

Object	Filter	Inst. Flux [10^{-13} erg cm^{-2} s^{-1}]	Med. flux [10^{-13} erg cm^{-2} s^{-1}]	Inst. Flux / Med. flux
ZTF18aavecmo	g	4.5	2.5	1.82
ZTF18aavecmo	r	4.3	2.6	1.67
ZTF18aavecmo	i	4.5	3.2	1.40
ZTF18abrwqpr	g	9.0	6.9	1.31
ZTF18abrwqpr	r	7.2	5.8	1.24
ZTF18abrwqpr	i	6.0	5.0	1.21
ZTF20aamoxyt	g	3.2	2.3	1.38
ZTF20aamoxyt	r	2.4	1.6	1.51
ZTF18abxrpgu	g	8.9	6.7	1.33
ZTF18abxrpgu	r	11.2	8.9	1.27
ZTF19aasfvqm	g	16.5	14.7	1.12
ZTF19aasfvqm	r	12.6	11.6	1.08
ZTF19aasfvqm	i	10.0	8.8	1.14

Table 3. Summary of the 5 AGN flares coincident with neutrinos, including the instantaneous flux during neutrino detection, median flux over the entire ZTF baseline, and the ratio of these values.
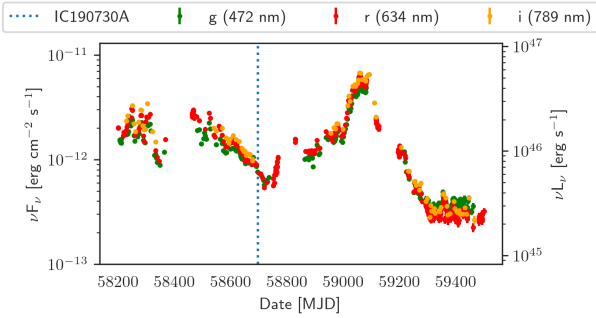

Figure 12. ZTF lightcurve of blazar PKS 1502+106. The arrival time of neutrino IC190730A is marked with the vertical dashed line.

Figure 13. ZTF lightcurve of blazar BZB J0955+3551. The arrival time of neutrino IC200107A is marked with the vertical dashed line.

tions, with both positive and negative flux changes relative to survey reference images.

The blazar lightcurve is shown in Figure 12, using data from science images with the ZTF forced photometry service (Masci et al. 2019). The neutrino arrival time is marked in blue. There was no significant flaring observed for this source coincident with the neutrino. The blazar at this point was dimmer than survey reference images, with the neutrino arriving during a year-long fading, and consequently was not selected by our follow-up pipeline as a possible counterpart. There is thus no evidence from the contemporaneous ZTF data to suggest a causal connection between IC190730A and PKS 1502+106, consistent with data from other observatories which did not see any evidence of short-term flaring (Franckowiak et al. 2020).

Data from the Owens Valley Radio Observatory (OVRO) did reveal that the radio flux was elevated in the months preceding the neutrino detection relative to the decade-long observation baseline, behaviour which has also been claimed for TXS 0506+056 and other neutrino-coincident blazars (Kiehlmann et al. 2019). Comprehensive time-dependent modelling has found that the detection of a neutrino alert from PKS 1502+106 is consistent with the multi-wavelength observations of this object, so a neutrino-blazar association is plausible but likely unrelated to the flaring activity (Rodrigues et al. 2021). In any case, the new optical data presented here can be used to further constrain such neutrino emission scenarios.

5.2 BZB J0955+3551

IC200107A was a high-energy neutrino reported by IceCube (Stein 2020a) which was later identified to be in spatial and temporal coincidence with a blazar undergoing a dramatic simultaneous X-ray flare (Krauss et al. 2020; Giommi et al. 2020c). The source BZB J0955+3551 (also known as 4FGL J0955.1+3551 and 3HSP J095507.9+355101), located at a redshift of 0.55703 (Paliya et al. 2020), belongs to the specific subclass of extreme blazars, which are characterised by synchrotron peaks at very high frequencies, which had been proposed as especially promising candidates of high-energy neutrinos (Padovani et al. 2016).

More comprehensive multi-frequency modelling has confirmed that the detection of a neutrino alert from an extreme blazar is plausible, though the simultaneous X-ray flare may not be directly related to the neutrino production (Paliya et al. 2020; Giommi et al. 2020b; Petropoulou et al. 2020). The ZTF lightcurve for BZB J0955+3551 is shown in Figure 13. There is no evidence of any optical flaring on short or long timescales coincident with the detection of IC200107A.

6 LIMITS ON NEUTRINO SOURCE POPULATIONS

With our program, we did not find any likely candidate counterparts from any population except TDEs. We can consider limits that can be placed on other potential sources of astrophysical neutrinos given

Event	P_{astro}	P_{obs}	$P_{astro} \times P_{obs}$
IC190503A	0.36	0.64	0.23
IC190619A	0.55	0.71	0.39
IC190730A	0.67	0.75	0.50
IC190922B	0.51	0.82	0.42
IC191001A	0.59	0.81	0.48
IC200107A	0.50	0.74	0.37
IC200109A	0.77	0.89	0.69
IC200117A	0.38	0.84	0.32
IC200512A	0.32	0.85	0.27
IC200530A	0.59	0.78	0.46
IC200620A	0.32	0.65	0.21
IC200916A	0.32	0.77	0.25
IC200926A	0.44	0.66	0.29
IC200929A	0.47	0.70	0.33
IC201007A	0.88	0.87	0.77
IC201021A	0.30	0.82	0.25
IC201130A	0.15	0.75	0.11
IC201209A	0.19	0.61	0.12
IC201222A	0.53	0.82	0.43
IC210210A	0.65	0.67	0.43
IC210510A	0.28	0.82	0.23
IC210629A	0.35	0.69	0.24
IC210811A	0.66	0.76	0.50
IC210922A	0.93	0.67	0.62

Table 4. Probability of finding a counterpart for each neutrino, assuming counterparts are sufficiently bright to be detected by our ZTF neutrino follow-up program.

the non-detections. These limits will clearly not apply for TDEs, because for this population probable counterparts were detected. It will however apply to other populations which would be detected by ZTF, provided at least one detection occurred within the 14 day window after neutrino arrival time. Our search has no requirement that an optical lightcurve peaks after the neutrino detection, so these limits also apply to older/fading transients.

For each neutrino, we can consider the probability that an astrophysical counterpart would be detected. A counterpart could only be detected if a given IceCube neutrino was astrophysical, with this as P_{astro} probability being reported by IceCube in GCN notices as the '*signalness*' parameter. For each neutrino that was indeed astrophysical, the source could only then be detected if it lay within the area observed by ZTF. We can estimate this probability, P_{obs}, by assuming that the 90% probability is uniformly distributed across the rectangle reported by IceCube, A_{IC}, such that:

$$P_{obs} = 0.9 \times \frac{A_{ZTF}}{A_{IC}} \tag{1}$$

where A_{ZTF} is the area observed by ZTF after accounting for detector chip gaps.

The probability to find an optical counterpart is then given by the joint probability that the neutrino is astrophysical, P_{astro}, that the astrophysical source lay in the observed ZTF area, P_{obs}, and the probability that a given counterpart would be detectable with our program $P_{detectable}$. The values of P_{astro} and P_{obs} for each alert are given in Table 4.

The detectable probability will depend on the selection efficiency, ϵ_{det}, of our program. This selection efficiency in turn depends on the apparent magnitude of the electromagnetic counterpart. Motivated by our classification efficiency in Figure 3, we assume completeness for objects brighter than 19.5 mag, and a classification efficiency of 68%
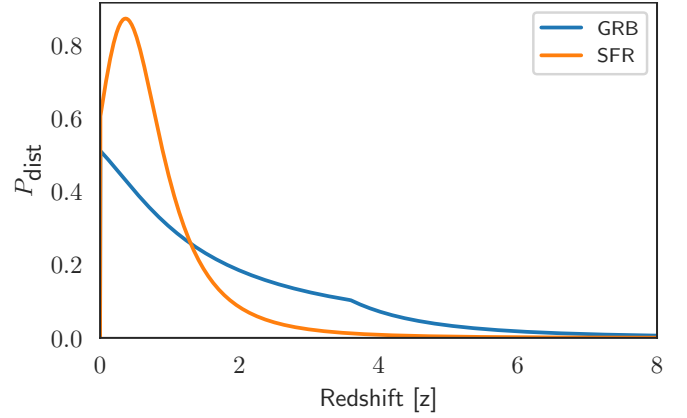

Figure 14. PDF for neutrino sources as a function of redshift, for both GRB-like and SFR-like source evolutions.

for objects fainter than this (this assumption is illustrated with the red dashed line in Figure 3). We additionally assume a conservative 95% detection efficiency for sources to be found by our pipeline, if said source was imaged by the camera. Chip gaps in the detector are already accounted for in Equation 1. Because the detection efficiency will decrease as the objects approach the ZTF limiting magnitude of 21.5 for 300s exposures, we neglect objects fainter than 21 mag in our calculation:

$$\epsilon_{selection}(m) = 0.95 \times \begin{cases} 1.00 & m \leq 19.5 \\ 0.68 & 19.5 \leq m \leq 21.0 \\ 0.00 & 21.0 \leq m \end{cases} \tag{2}$$

The fraction of astrophysical neutrino sources that are detected by our program will depend on the properties of a given population. For a power law neutrino spectrum, the neutrino flux at Earth for a transient population as a function of redshift is proportional to:

$$\frac{dF(z)}{dz} \propto \left[(1+z)^{2-\gamma} \times \frac{R(z)}{4\pi D_L^2} \right] \frac{dV_C}{dz} \tag{3}$$

where γ is the intrinsic neutrino spectral index such that $\frac{dN_\nu}{dE} \propto E^{-\gamma}$, $R(z) = \rho(z)/\rho(0)$ is the normalised source redshift evolution for a population with rate $\rho(z)$, D_L is the luminosity distance and V_C is the comoving volume. The neutrino flux scaling is thus independent of the local rate $\rho(0)$ for a given transient population. By normalising Equation 3, we can derive a probability density function (PDF) for the redshift of detected neutrinos:

$$P_{dist}(z) = \frac{dF(z)}{dz} \left/ \left(\int_0^\infty \frac{dF(z)}{dz} dz \right) \right. \tag{4}$$

PDFs for $P_{dist}(z)$, calculated using the *flarestack* code (Stein et al. 2020a), are shown in Figure 14 for redshift evolutions from a 'GRB-like' population (Lien et al. 2014) and from a Star-Formation-Rate population ('SFR-like') (Strolger et al. 2015). It can be seen in Figure 14 that GRB-like populations tend to be at greater distances than SFR-like ones, with GRB-like neutrinos being emitted from a median redshift of z = 1.34, whereas SFR-like neutrinos would have a median distance of z = 0.64. This has a direct impact on the population properties compatible with our limits, because a neutrino population dominated by nearby sources will generally produce counterparts with brighter apparent magnitudes.
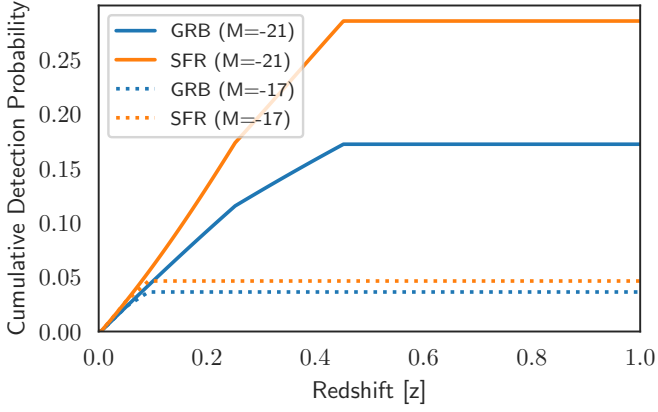
Figure 15. Cumulative counterpart detection probability as a function of redshift.
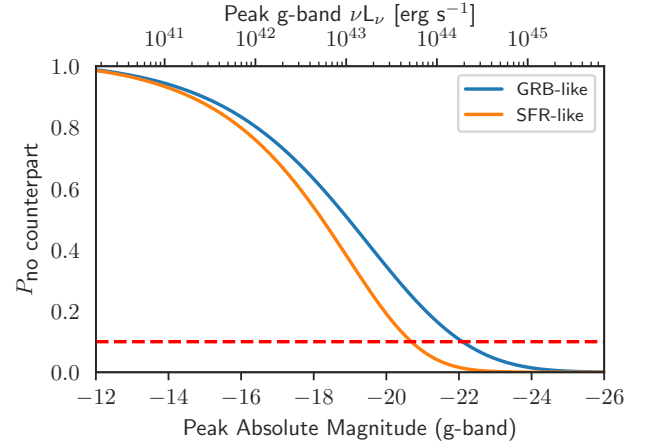

Figure 16. Probability of detecting no counterpart as a function of absolute magnitude for $f = 1$. The dotted line corresponds to 90% confidence.

For a given source evolution, the probability of detecting a counterpart will then ultimately depend on the underlying luminosity function of the population. For an absolute magnitude, M, the counterpart detection probability is equal to the integrated product of the probability that a counterpart has a given redshift, $P_{dist}(z)$, and the detection efficiency of our program for the apparent magnitude, $m(M, z)$, corresponding to that redshift:

$$P_{detectable}(M) = \int_0^\infty \left[\epsilon_{det}(m(M, z)) \times P_{dist}(z) \right] dz \quad (5)$$

The impact of different evolutions and absolute magnitudes can be seen in Figure 15. For sources with an absolute magnitude of -21, our program would be sensitive to counterparts up to a redshift of $z \approx 0.45$, beyond which $m > 21$ so $\epsilon_{selection} = 0$. For an SFR-like evolution, this would correspond to $P_{detectable}(-21) = 26\%$, but for the higher-$z$ GRB-like neutrino distribution, we would instead find $P_{detectable} = 16\%$. For a fainter absolute magnitude of -17, our program would probe a much smaller volume up to redshift $z \approx 0.1$, so then $P_{detectable}$ would be 5% and 4% for SFR-like and GRB-like populations respectively.

Combining these values, the joint probability for us to find a counterpart during a follow-up campaign is given by:

$$P_{find}(f, M) = P_{astro} \times P_{obs} \times P_{detectable}(M) \times f(M) \quad (6)$$

where f is the fraction of astrophysical neutrino sources with an absolute magnitude equal to or brighter than M. The probability that no counterpart was detected in any of our 24 follow-up observations is then given by:

$$P_{no\_counterpart}(M, f) = \prod_{i=1}^{24} \left(1 - P_{find, i}(M, f) \right) \quad (7)$$

The probability of no counterpart detection is given in Figure 16 as a function of M. The results of our program strongly disfavour scenarios where all neutrino sources have bright absolute magnitudes. The horizontal dashed line in Figure 16 represents a 10% chance of non-detection, and thus a 90% confidence limit. We can use this threshold to set a limit on the luminosity function of neutrino sources, by choosing the appropriate fraction f such that $P_{no\ counterpart}(M, f) > 0.1$
.

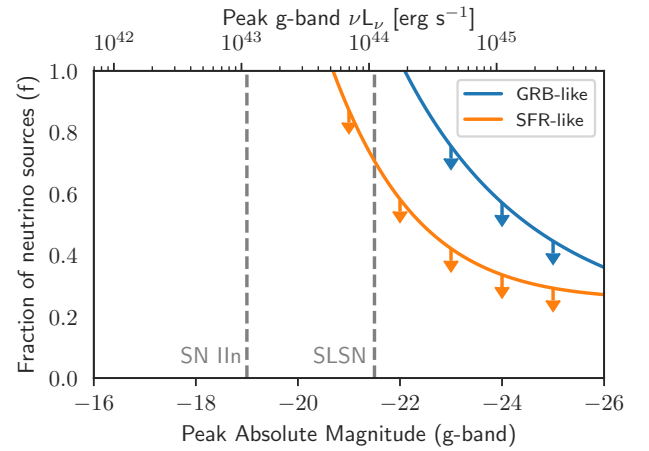These constraints on $f(M)$ at 90% CL are illustrated in Figure 17,

Figure 17. Upper limits (90% CL) on the luminosity function of neutrino sources.

for the two source evolutions. These are generic constraints on the underlying luminosity function of neutrino sources, and are agnostic to the actual nature of the neutrino sources which follow the redshift evolutions. They constrain the aggregate neutrino flux emitted by e.g. a SFR-like population, and thus apply equally well to a composite neutrino flux with e.g. multiple SFR-like neutrino populations. To the best knowledge of the authors, this is the first time generic constraints on the optical luminosity function of neutrino sources have been derived, though a similar procedure has already been used to derive limits from optical searches for counterparts to gravitational waves (Kasliwal et al. 2020). One novel consequence of these general limits are the first observational constraints on the contribution of the brightest superluminous supernova to the diffuse neutrino flux, under the assumption these trace the star formation rate. Objects brighter than an absolute magnitude of -22 can contribute no more than 58% of the total astrophysical neutrino alerts if SFR-like. It should be noted that these values do not account for the impact of dust extinction, which would shift the curves in Figure 17 rightwards to higher luminosities. However, we do not expect that this would significantly impact the results presented here.

It should be noted that these limits assume that a given transient could pass our selection criteria outlined in Section 2, and therefore do not apply to extremely rapid transients such as GRB afterglows, which peak and fade on timescales $\lesssim 1$ day. Such objects are not well
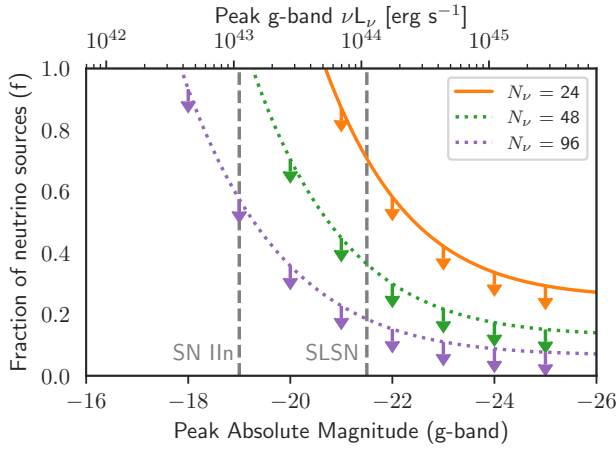
Figure 18. Upper limits (90% CL) on the luminosity function of neutrino sources for an SFR-like evolution that would be derived for a ZTF neutrino sample that was twice (N_ν=48) or four times (N_ν=96) the size of the sample presented here.

Figure 19. Upper limits (90% CL) on the luminosity function for an SFR-like population with our sample of 24 observed neutrino alert and our classification efficiency (ZTF ν follow-up), and limits that would be obtained for a comparable neutrino follow-up program with the upcoming Rubin Observatory.

captured by the ZTF public survey cadence or our typical neutrino follow-up observation cadence, and are unlikely to be detected multiple times in order to pass our selection criteria, so our detection efficiency will be somewhat lower.

7 CONCLUSIONS

The ZTF neutrino follow-up program coincided with the introduction of the upgraded IceCube alert selection, yielding one unretracted alert every 2 weeks and one ZTF follow-up campaign every 4 weeks on average. The program resulted in the identification of two probable neutrino sources (Stein et al. 2021b; Reusch et al. 2021a), and the first limits on the optical luminosity function of neutrino sources.

Though the limits presented here constrain only the very brightest transients such as superluminous supernovae (SLSNe), they will continue to become more stringent over time if no new counterparts are identified. As can be seen in Figure 18, extrapolating our analysis to a neutrino sample that was twice or four times as large would lead to substantially more constraining limits, and will be achieved on the present trajectory with 2 or 6 additional years of observations.

Although the data analysis presented considered candidates detected up to 14 days after neutrino detection, our early real-time counterpart searches generally focussed on counterparts detected in the ToO observations scheduled for the first two nights after neutrino detection. Motivated by the systematic analysis performed here, and to improve sensitivity to time-delayed optical signatures such as neutrino emission from choked jets, we have modified our ToO observation strategy to better cover a range of transient timescales. We now trigger deep 300s in *g* and *r* band on the first night of observations to obtain deep upper limits or faint detections, and to additionally yield colour information for any active transient. However, we replaced our second pair of 300s exposures with a series of 30s exposures spread over subsequent nights, to complement the public survey and ensure good coverage of the photometric evolution of candidates. Forced photometry is only possible for images from the public survey after they have been published as part of the regular ZTF Data Releases, but with this ToO monitoring we can perform forced photometry analysis in real time (Reusch 2020). We can also better prioritise spectroscopic follow-up with photometric classification.

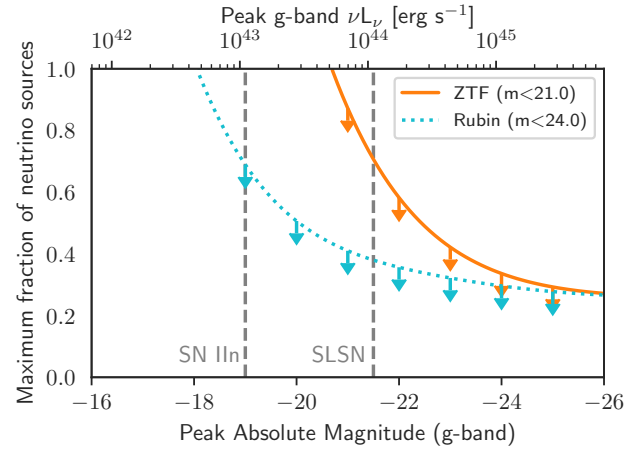One shortcoming of the ZTF program thus far has been the rel-

atively poor sensitivity to very rapid transients such as GRB afterglows, owing to the median latency of 12.8 hours to first coverage. We plan to implement automated triggering with ZTF, similar to that operated by other observatories such as ASAS-SN (Necker et al. in prep), enabling low-latency observations for at least some favourable neutrino alerts with appropriate accessibility. Dedicated analysis of low-latency follow-up campaigns would yield more stringent constraints on GRB afterglows as neutrino sources.

The results and analysis presented here can serve as a pathfinder for future triggered neutrino follow-up programs with wide-field instruments. In particular, ToO observations with the upcoming Vera C. Rubin Observatory would offer an unprecedented opportunity to probe neutrino sources to much higher redshifts (Ivezić et al. 2019). Multi-band observation coverage would enable photometric classification of many candidates, substantially extending the classification efficiency presented in Figure 3 to much greater depths. An illustration of this is presented in Figure 19, assuming that the same neutrino sample in Table 1 had instead been observed with the Rubin Observatory. For a comparable 60% classification efficiency down to 24th mag, the corresponding limits on the neutrino luminosity function would be much more constraining for lower magnitudes. However, for very luminous neutrino sources, the performance of both surveys for such a neutrino sample would be comparable. Given that there are only expected to be ~12 astrophysical neutrinos in our sample, observations will never be able to overcome the 90% limit from Poisson counting statistics even if they had a perfect 100% efficiency. Instead, as seen in Figure 18, only larger neutrino samples can enable stricter limits on bright sources.

Beyond optical observatories, similar electromagnetic neutrino follow-up programs are planned for telescopes currently under construction. These include near infra-red (NIR) wavelengths with WINTER (Lourie et al. 2020; Frostig et al. 2020), at ultra-violet (UV) wavelengths with ULTRASAT (Sagiv et al. 2014), and in gamma-rays with CTA (Cherenkov Telescope Array Consortium et al. 2019; Carosi et al. 2021). These new instruments, in concert with the continuation of existing follow-up programs, will enable us to study the dynamic neutrino sky across the entire electromagnetic spectrum.

ACKNOWLEDGEMENTS

DATA AVAILABILITY

The data presented here, and the Python analysis code used to generate the figures and key results, will be provided by the authors upon reasonable request.

REFERENCES

Aartsen M. G., et al., 2015, ApJ, 811, 52
Aartsen M. G., et al., 2017, Astroparticle Physics, 92, 30
Aartsen M. G., et al., 2020, Phys. Rev. Lett., 124, 051103
Abbasi R., et al., 2021, arXiv e-prints, p. arXiv:2111.10169
Abolfathi B., et al., 2018, ApJS, 235, 42
Albareti F. D., et al., 2017, ApJS, 233, 25
Astropy Collaboration et al., 2013, A&A, 558, A33
Astropy Collaboration et al., 2018, AJ, 156, 123
Barbon R., Benetti S., Cappellaro E., Patat F., Turatto M., Iijima T., 1995, A&AS, 110, 513
Bednarek W., Protheroe R. J., 1999, MNRAS, 302, 373
Bellm E. C., et al., 2019a, PASP, 131, 018002
Bellm E. C., et al., 2019b, PASP, 131, 068003
Blaufuss E., 2018a, GCN Circular, 23214
Blaufuss E., 2018b, GCN Circular, 23375
Blaufuss E., 2018c, GCN Circular, 23398
Blaufuss E., 2019a, GCN Circular, 23785
Blaufuss E., 2019b, GCN Circular, 23876
Blaufuss E., 2019c, GCN Circular, 24378
Blaufuss E., 2019d, GCN Circular, 24674
Blaufuss E., 2019e, GCN Circular, 24854
Blaufuss E., 2019f, GCN Circular, 24910
Blaufuss E., 2019g, GCN Circular, 25057
Blaufuss E., 2019h, GCN Circular, 25806
Blaufuss E., 2019i, GCN Circular, 26258
Blaufuss E., 2019j, GCN Circular, 26276
Blaufuss E., 2020a, GCN Circular, 27612
Blaufuss E., 2020b, GCN Circular, 27787
Blaufuss E., 2020c, GCN Circular, 27941
Blaufuss E., 2020d, GCN Circular, 28163
Blaufuss E., 2020e, GCN Circular, 28433
Blaufuss E., 2020f, GCN Circular, 28509
Blaufuss E., 2020g, GCN Circular, 28616
Blaufuss E., 2020h, GCN Circular, 28887
Blaufuss E., 2020i, GCN Circular, 28892
Blaufuss E., 2020j, GCN Circular, 29102
Blaufuss E., 2020k, GCN Circular, 29120
Blaufuss E., 2021a, GCN Circular, 29506
Blaufuss E., 2021b, GCN Circular, 31249
Blaufuss E., Kintscher T., Lu L., Tung C. F., 2019, in 36th International Cosmic Ray Conference (ICRC2019). p. 1021 (arXiv:1908.04884)
Blondin S., Tonry J. L., 2007, ApJ, 666, 1024
Carosi A., et al., 2021, arXiv e-prints, p. arXiv:2108.04309
Cherenkov Telescope Array Consortium et al., 2019, Science with the Cherenkov Telescope Array, doi:10.1142/10986.
Dekany R., et al., 2020, PASP, 132, 038001
Evans P. A., et al., 2015, MNRAS, 448, 2210
Farrar G. R., Gruzinov A., 2009, ApJ, 693, 329
Ferrigno C., et al., 2021, New Astron. Rev., 92, 101595
Flesch E. W., 2021, arXiv e-prints, p. arXiv:2105.12985
Franckowiak A., et al., 2020, ApJ, 893, 162
Fremling C., et al., 2020, ApJ, 895, 32
Frostig D., et al., 2020, in Society of Photo-Optical Instrumentation Engineers (SPIE) Conference Series. p. 1144767 (arXiv:2105.01219), doi:10.1117/12.2562842
Gaia Collaboration et al., 2018, A&A, 616, A1
Galama T. J., et al., 1998, Nature, 395, 670
Garrappa S., Buson S., Franckowiak A., Giroletti M., Liodakis I., Nanci C., 2021, PoS, ICRC2021, 956

Ginsburg A., et al., 2019, AJ, 157, 98

Giommi P., Glauch T., Padovani P., Resconi E., Turcati A., Chang Y. L., 2020a, MNRAS, 497, 865

Giommi P., Padovani P., Oikonomou F., Glauch T., Paiano S., Resconi E., 2020b, A&A, 640, L4

Giommi P., Glauch T., Resconi E., 2020c, The Astronomer's Telegram, 13394, 1

Graham M. J., et al., 2019, PASP, 131, 078001

Guillochon J., Nicholl M., Villar V. A., Mockler B., Narayan G., Mandel K. S., Berger E., Williams P. K. G., 2018, ApJS, 236, 6

Hayasaki K., 2021, Nature Astronomy, 5, 436

Holmbo S., et al., 2019, The Astronomer's Telegram, 12661

IceCube Collaboration 2013, Science, 342, 1242856

IceCube Collaboration et al., 2018, Science, 361, eaat1378

Ivezić Ž., et al., 2019, ApJ, 873, 111

Kadler M., et al., 2021, arXiv e-prints, p. arXiv:2108.00383

Kasliwal M. M., et al., 2020, ApJ, 905, 145

Kiehlmann S., Hovatta T., Kadler M., Max-Moerbeck W., Readhead A. C. S., 2019, The Astronomer's Telegram, 12996

Kopper C., 2018, GCN Circular, 22669

Kopper C., 2019a, GCN Circular, 23605

Kopper C., 2019b, GCN Circular, 24028

Kopper C., 2019c, GCN Circular, 24392

Kowalski M., Mohr A., 2007, Astroparticle Physics, 27, 533

Krauss F., Gregoire T., Fox D. B., Kennea J., Evans P., 2020, The Astronomer's Telegram, 13395, 1

Lagunas Gualda C., 2020a, GCN Circular, 26802

Lagunas Gualda C., 2020b, GCN Circular, 26832

Lagunas Gualda C., 2020c, GCN Circular, 27719

Lagunas Gualda C., 2020d, GCN Circular, 27950

Lagunas Gualda C., 2020e, GCN Circular, 28411

Lagunas Gualda C., 2020f, GCN Circular, 28468

Lagunas Gualda C., 2020g, GCN Circular, 28504

Lagunas Gualda C., 2020h, GCN Circular, 28532

Lagunas Gualda C., 2020i, GCN Circular, 28715

Lagunas Gualda C., 2020j, GCN Circular, 28889

Lagunas Gualda C., 2020k, GCN Circular, 28927

Lagunas Gualda C., 2020l, GCN Circular, 28969

Lagunas Gualda C., 2020m, GCN Circular, 29012

Lagunas Gualda C., 2021a, GCN Circular, 29454

Lagunas Gualda C., 2021b, GCN Circular, 30153

Lagunas Gualda C., 2021c, GCN Circular, 30468

Lagunas Gualda C., 2021d, GCN Circular, 31085

Lagunas Gualda C., 2021e, GCN Circular, 31126

Lagunas Gualda C., Ashida Y., Sharma A., Thomas H., 2021, PoS, ICRC2021, 1045

Lien A., Sakamoto T., Gehrels N., Palmer D. M., Barthelmy S. D., Graziani C., Cannizzo J. K., 2014, ApJ, 783, 24

Lincetto M., 2021a, GCN Circular, 30862

Lincetto M., 2021b, GCN Circular, 30957

Lincetto M., 2021c, GCN Circular, 31241

Lourie N. P., et al., 2020, in Society of Photo-Optical Instrumentation Engineers (SPIE) Conference Series. p. 114479K (arXiv:2102.01109), doi:10.1117/12.2561210

Lucarelli F., et al., 2019, ApJ, 870, 136

Lyman J. D., Bersier D., James P. A., Mazzali P. A., Eldridge J. J., Fraser M., Pian E., 2016, MNRAS, 457, 328

Mannheim K., 1993, A&A, 269, 67

Masci F. J., et al., 2019, PASP, 131, 018003

Morgan R., et al., 2019, ApJ, 883, 125

Murase K., Thompson T. A., Lacki B. C., Beacom J. F., 2011, Phys. Rev. D, 84, 043003

Nakar E., 2015, ApJ, 807, 172

Necker J., Stein R., Weimann S., Reusch S., Franckowiak A., 2021, GCN Circular, 30349

Necker J., de Jaeger T., Stein R., Franckowiak A., Shappee B., Kowalski M., et al., in prep., ASAS-SN follow-up of IceCube high-energy neutrino alerts

Nordin J., et al., 2019, A&A, 631, A147

Oke J. B., et al., 1995, PASP, 107, 375

Padovani P., Resconi E., Giommi P., Arsioli B., Chang Y. L., 2016, MNRAS, 457, 3582

Paliya V. S., Böttcher M., Olmo-García A., Domínguez A., Gil de Paz A., Franckowiak A., Garrappa S., Stein R., 2020, ApJ, 902, 29

Pan-Starrs Collaboration et al., 2019, A&A, 626, A117

Pastorello A., et al., 2006, MNRAS, 370, 1752

Patterson M. T., et al., 2019, PASP, 131, 018001

Perley D. A., et al., 2020, ApJ, 904, 35

Petropoulou M., Oikonomou F., Mastichiadis A., Murase K., Padovani P., Vasilopoulos G., Giommi P., 2020, ApJ, 899, 113

Plavin A., Kovalev Y. Y., Kovalev Y. A., Troitsky S., 2020, ApJ, 894, 101

Plavin A. V., Kovalev Y. Y., Kovalev Y. A., Troitsky S. V., 2021, ApJ, 908, 157

Reguitti A., et al., 2019, The Astronomer's Telegram, 13133

Reusch S., 2020, simeonreusch/ztffps: Release (3), doi:10.5281/zenodo.4049711, https://doi.org/10.5281/zenodo.4049711

Reusch S., Stein R., 2020a, GCN Circular, 26747

Reusch S., Stein R., 2020b, GCN Circular, 26813

Reusch S., Stein R., 2020c, GCN Circular, 26816

Reusch S., Stein R., Franckowiak A., 2020a, GCN Circular, 27721

Reusch S., Stein R., Franckowiak A., Gezari S., 2020b, GCN Circular, 27872

Reusch S., Stein R., Franckowiak A., Sollerman J., Schweyer T., Barbarino C., 2020c, GCN Circular, 27910

Reusch S., Stein R., Franckowiak A., Necker J., Sollerman J., Barbarino C., Schweyer T., 2020d, GCN Circular, 27980

Reusch S., Stein R., Franckowiack A., 2020e, GCN Circular, 28005

Reusch S., Stein R., Franckowiak A., Andreoni I., Coughlin M., 2020f, GCN Circular, 28441

Reusch S., Stein R., Franckowiak A., Schulze S., Sollerman J., 2020g, GCN Circular, 28465

Reusch S., Stein R., Weimann S., Franckowiak A., 2020h, GCN Circular, 28520

Reusch S., Weimann S., Stein R., Franckowiak A., 2020i, GCN Circular, 28609

Reusch S., Weimann S., Stein R., Franckowiak A., 2020j, GCN Circular, 29031

Reusch S., et al., 2021a, arXiv e-prints, p. arXiv:2111.09390

Reusch S., Weimann S., Stein R., Coughlin M., Franckowiak A., 2021b, GCN Circular, 29461

Rodrigues X., Garrappa S., Gao S., Paliya V. S., Franckowiak A., Winter W., 2021, ApJ, 912, 54

Sagiv I., et al., 2014, AJ, 147, 79

Santander M., 2019a, GCN Circular, 24981

Santander M., 2019b, GCN Circular, 25402

Santander M., 2019c, GCN Circular, 26620

Santander M., 2020a, GCN Circular, 27651

Santander M., 2020b, GCN Circular, 27997

Santander M., 2020c, GCN Circular, 28575

Santander M., 2021a, GCN Circular, 29688

Santander M., 2021b, GCN Circular, 29951

Santander M., 2021c, GCN Circular, 29976

Santander M., 2021d, GCN Circular, 30026

Santander M., 2021e, GCN Circular, 30056

Santander M., 2021f, GCN Circular, 30342

Santander M., 2021g, GCN Circular, 30559

Santander M., 2021h, GCN Circular, 30627

Santander M., 2021i, GCN Circular, 31093

Santander M., 2021j, GCN Circular, 31110

Santander M., 2021k, GCN Circular, 31195

Satalecka K., Bernardini E., Dorner D., Kukec Mezek G., Jin W., 2021, arXiv e-prints, p. arXiv:2109.04350

Senno N., Murase K., Mészáros P., 2016, Phys. Rev. D, 93, 083003

Stein R., 2019a, GCN Circular, 25225

Stein R., 2019b, GCN Circular, 25802

Stein R., 2019c, GCN Circular, 25913
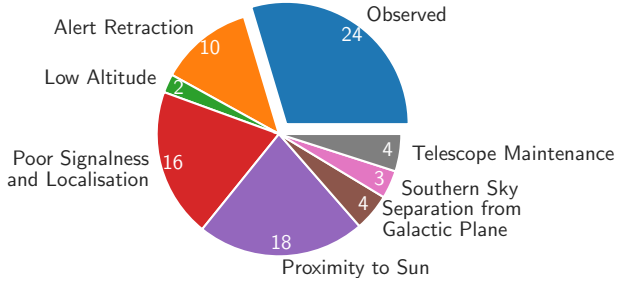
Figure A1. Breakdown of the neutrino follow-up program, as of 2021 Dec 31.

Those alerts not observed by ZTF are summarised in Table A1. Of those 57 alerts not followed up, the primary reasons were proximity to the Sun (18/55), alerts with poor localisation and low astrophysical probability (16/55) and alert retraction (10/55). The full breakdown of neutrino observations statistics can be seen in Figure A1.

This paper has been typeset from a TEX/LATEX file prepared by the author.

Stein R., 2019d, GCN Circular, 26341

Stein R., 2019e, GCN Circular, 26435

Stein R., 2020a, GCN Circular, 26655

Stein R., 2020b, GCN Circular, 26696

Stein R., 2020c, GCN Circular, 27235

Stein R., 2020d, GCN Circular, 27534

Stein R., 2020e, GCN Circular, 27865

Stein R., 2020f, GCN Circular, 28210

Stein R., Reusch S., 2020, GCN Circular, 26667

Stein R., et al., 2019a, The Astronomer's Telegram, 12730

Stein R., et al., 2019b, The Astronomer's Telegram, 12879

Stein R., Franckowiak A., Kasliwal M. M., Andreoni I., Coughlin M., Singer L. P., Masci F., van Velzen S., 2019c, The Astronomer's Telegram, 12974

Stein R., Franckowiak A., Kowalski M., Kasliwal M., 2019d, GCN Circular, 25824

Stein R., Franckowiak A., Necker J., Gezari S., van Velzen S., 2019e, GCN Circular, 25929

Stein R., Necker J., Bradascio F., simonegarrappa 2020a, icecube/flarestack, doi:10.5281/zenodo.3619383, https://doi.org/10.5281/zenodo.3619383

Stein R., Reusch S., Weimann S., Coughlin M., 2020b, GCN Circular, 28757

Stein R., Weimann S., Reusch S., Franckowiak A., 2020c, GCN Circular, 29172

Stein R., Reusch S., Necker J., 2021a, desy-multimessenger/nuztf: v2.1.0 Release, doi:10.5281/zenodo.5217976, https://doi.org/10.5281/zenodo.5217976

Stein R., et al., 2021b, Nature Astronomy, 5, 510

Stein R., Weimann S., Necker J., Reusch S., Franckowiak A., Zwicky Transient Facility Growth Collaboration 2021c, GCN Circular, 29999

Stein R., Weimann S., Reusch S., Necker J., Franckowiak A., Coughlin M., Zwicky Transient Facility collaboration Global Relay of Observatories Watching Transients Happen Collaboration 2021d, GCN Circular, 30644

Stern D., et al., 2012, ApJ, 753, 30

Stoughton C., et al., 2002, AJ, 123, 485

Strolger L.-G., et al., 2015, ApJ, 813, 93

Strotjohann N. L., Kowalski M., Franckowiak A., 2019, A&A, 622, L9

Taboada I., 2018, GCN Circular, 23338

Taboada I., 2019, GCN Circular, 23918

Taubenberger S., et al., 2006, MNRAS, 371, 1459

Waxman E., Bahcall J., 1997, Phys. Rev. Lett., 78, 2292

Weimann S., Stein R., Reusch S., Franckowiak A., 2020a, GCN Circular, 28551

Weimann S., Stein R., Reusch S., Franckowiak A., 2020b, GCN Circular, 28989

Weimann S., Reusch S., Necker J., Stein R., Franckowiak A., Zwicky Transient Facility Growth Collaboration 2021, GCN Circular, 30870

Wright E. L., et al., 2010, AJ, 140, 1868

van Velzen S., et al., 2021, arXiv e-prints, p. arXiv:2111.09391

Cause	Events
Alert Retraction	IC180423A (Kopper 2018)
	IC181031A (Blaufuss 2018c)
	IC190205A (Blaufuss 2019b)
	IC190529A (Blaufuss 2019d)
	IC200120A (Lagunas Gualda 2020b)
	IC200728A (Blaufuss 2020d)
	IC201115B (Blaufuss 2020i)
	IC210213A (Blaufuss 2021a)
	IC210322A (Santander 2021a)
	IC210519A (Santander 2021e)
Proximity to Sun	IC180908A (Blaufuss 2018a)
	IC181014A (Taboada 2018)
	IC190124A (Blaufuss 2019a)
	IC190704A (Santander 2019a)
	IC190712A (Blaufuss 2019g)
	IC190819A (Santander 2019b)
	IC191119A (Blaufuss 2019i)
	IC200227A (Stein 2020c)
	IC200421A (Blaufuss 2020a)
	IC200615A (Lagunas Gualda 2020d)
	IC200806A (Stein 2020f)
	IC200921A (Lagunas Gualda 2020f)
	IC200926B (Blaufuss 2020f)
	IC201014A (Blaufuss 2020g)
	IC201115A (Lagunas Gualda 2020j)
	IC201221A (Blaufuss 2020j)
	IC211117A (Santander 2021i)
	IC211123A (Santander 2021j)
Low Altitude	IC191215A (Stein 2019e)
	IC211023A (Lincetto 2021b)
Southern Sky	IC190104A (Kopper 2019a)
	IC190331A (Kopper 2019b)
	IC190504A (Kopper 2019c)
Separation from Galactic Plane	IC201114A (Blaufuss 2020h)
	IC201120A (Lagunas Gualda 2020k)
	IC210516A (Santander 2021d)
	IC210730A (Santander 2021g)
Poor Signalness and Localisation	IC190221A (Taboada 2019)
	IC190629A (Blaufuss 2019f)
	IC190922A (Stein 2019b)
	IC191122A (Blaufuss 2019j)
	IC191204A (Stein 2019d)
	IC191231A (Santander 2019c)
	IC200410A (Stein 2020d)
	IC200425A (Santander 2020a)
	IC200523A (Blaufuss 2020b)
	IC200614A (Blaufuss 2020c)
	IC200911A (Lagunas Gualda 2020e)
	IC210503A (Santander 2021b)
	IC210608A (Lagunas Gualda 2021b)
	IC210717A (Lagunas Gualda 2021c)
	IC211125A (Lagunas Gualda 2021e)
	IC211216A (Lincetto 2021c)
Telescope Maintenance	IC181023A (Blaufuss 2018b)
	IC211116A (Lagunas Gualda 2021d)
	IC211208A (Santander 2021k)
	IC211216B (Blaufuss 2021b)

Table A1. Summary of the 57 neutrino alerts that were not followed up by ZTF since survey start on 2018 March 20.

ZTF Name	IAU Name	Classification	Peak Magnitude
ZTF19aatqcwq	–	AGN Variability	20.6 (g)
ZTF19aatqlwq	–	AGN Variability	21.2 (r)

Table A2. Candidates for IC190503A.

ZTF Name	IAU Name	Classification	Peak Magnitude
ZTF18abolwbb	–	AGN Variability	19.4 (r)
ZTF18abueqkl	AT2020kqj	AGN Variability	19.3 (g)
ZTF18acehkni	–	AGN Variability	19.4 (r)
ZTF18actxchc	–	AGN Variability	18.0 (g)
ZTF19aadaszg	SN2019rg	SN Ia	15.9 (r)
ZTF19aawnawu	–	AGN Variability	20.0 (g)
ZTF19aaycone	–	AGN Variability	17.9 (g)
ZTF19aaycool	–	AGN Variability	20.3 (g)
ZTF19aaycosc	–	AGN Variability	19.3 (r)
ZTF19aaycoxd	–	AGN Variability	20.3 (g)
ZTF19abahiwr	AT2019izf	Unclassified	19.5 (r)
ZTF19abahiya	–	Unclassified	19.6 (r)
ZTF19abahizn	–	AGN Variability	19.7 (g)
ZTF19abahjcp	–	AGN Variability	20.2 (g)
ZTF19abahlep	–	Unclassified	20.8 (r)
ZTF19abahlka	–	AGN Variability	19.8 (i)
ZTF19abajnby	–	AGN Variability	20.0 (r)

Table A3. Candidates for IC190619A.

ZTF Name	IAU Name	Classification	Peak Magnitude
ZTF19aanlzzk	–	Artefact	13.8 (g)

Table A4. Candidates for IC190730A.

ZTF Name	IAU Name	Classification	Peak Magnitude
ZTF18acekfly	AT2019kkd	AGN Variability	18.5 (r)
ZTF19abcejyp	AT2019kkp	AGN Variability	19.3 (r)
ZTF19abxtupj	AT 2019pqh	SN II/IIb	20.3 (r)

Table A5. Candidates for IC190922B.

ZTF Name	IAU Name	Classification	Peak Magnitude
ZTF18ablvxkp	–	AGN Variability	19.3 (r)
ZTF18absoqfm	–	AGN Variability	19.0 (g)
ZTF19aapreis	AT2019dsg	TDE	17.8 (g)
ZTF19abassjx	–	AGN Variability	19.4 (i)
ZTF19abcdynm	–	AGN Variability	20.5 (g)
ZTF19abexshr	–	AGN Variability	20.2 (r)
ZTF19abjfikj	–	AGN Variability	20.9 (g)
ZTF19abjflnc	–	AGN Variability	19.2 (i)
ZTF19abjflrg	–	AGN Variability	21.3 (g)
ZTF19abjfmem	–	AGN Variability	21.5 (g)
ZTF19abwaurq	–	Unclassified	19.5 (r)
ZTF19abzkexb	SN2019qhl	SN Ia	18.9 (g)
ZTF19acbpqfn	AT2019rsj	Unclassified	20.4 (g)
ZTF19acbpqui	–	Unclassified	20.5 (g)
ZTF19acbwpqs	–	AGN Variability	19.9 (g)
ZTF19acbxahc	–	Unclassified	21.1 (g)
ZTF19acbxanz	–	Unclassified	20.6 (r)
ZTF19acbxaqj	–	Unclassified	20.5 (r)
ZTF19acbxauk	–	Unclassified	20.8 (g)
ZTF19acbxbjq	AT2019rsk	Unclassified	20.3 (g)
ZTF19accnqlc	–	Unclassified	20.2 (r)

Table A6. Candidates for IC191001A.

ZTF Name	IAU Name	Classification	Peak Magnitude
ZTF18aaidhnq	–	AGN Variability	18.1 (r)
ZTF18aceykyg	–	AGN Variability	19.0 (g)
ZTF18adgvgdk	–	AGN Variability	19.3 (g)
ZTF19aangwsm	–	Artefact	19.8 (g)
ZTF19aapsgtb	–	AGN Variability	18.8 (r)
ZTF19aarohku	–	AGN Variability	19.8 (r)
ZTF19acmwlds	AT 2019yfm	Unclassified	19.7 (g)
ZTF19adcdxgc	–	AGN Variability	19.6 (g)
ZTF20aaeunmm	–	AGN Variability	20.4 (g)
ZTF20aaeuufe	AT 2019yii	Unclassified	20.4 (r)
ZTF20aaevfrv	–	Star	20.7 (g)
ZTF20aaevfth	AT 2020ux	Unclassified	21.2 (g)
ZTF20aaevfwa	AT 2019zxa	Unclassified	20.6 (r)
ZTF20aaevgvt	AT 2020uw	Artefact	20.5 (r)
ZTF20aagvvve	–	Artefact	19.7 (r)
ZTF20aagvvvh	–	Artefact	19.8 (r)
ZTF20aagvvvk	–	Artefact	19.9 (r)
ZTF20aagvvvn	–	Artefact	20.0 (r)
ZTF20aagwcup	AT2020dtc	Artefact	19.9 (r)
ZTF20aagwcuq	–	Unclassified	20.0 (r)
ZTF20aagwcuu	–	Unclassified	20.0 (r)
ZTF20aagwcuv	–	Unclassified	19.9 (r)
ZTF20aagxfta	–	Unclassified	19.9 (g)

Table A7. Candidates for IC200109A.

ZTF Name	IAU Name	Classification	Peak Magnitude
ZTF19acxopgh	AT 2019zyu	Unclassified	19.4 (r)
ZTF19adceqeb	–	AGN Variability	19.6 (g)
ZTF20aacztcp	AT2020ko	AGN Variability	19.0 (r)
ZTF20aaglixd	AT 2020agt	Unclassified	21.2 (g)

Table A8. Candidates for IC200117A.

ZTF Name	IAU Name	Classification	Peak Magnitude
ZTF18aazvbyj	–	Star	17.5 (r)
ZTF18abjnqos	–	Star	12.9 (r)
ZTF18abmfxbh	–	Artefact	17.5 (r)
ZTF18abmfzmm	–	Artefact	17.1 (r)
ZTF19acgpzgi	–	Artefact	15.5 (g)
ZTF20aazqsfe	–	Star	19.6 (g)

Table A9. Candidates for IC200512A.

ZTF Name	IAU Name	Classification	Peak Magnitude
ZTF18aaimsgg	AT2018lnq	Artefact	16.6 (r)
ZTF18aamjqes	AT2020llg	AGN Variability	16.9 (r)
ZTF18aaneyxs	–	Artefact	14.6 (r)
ZTF18aavecmo	AT2020llh	AGN Flare	19.6 (i)
ZTF18aazkjyd	–	Artefact	14.7 (r)
ZTF18abrwqpr	AT2020lli	AGN Flare	19.6 (g)
ZTF19aaonfhr	AT2020llj	AGN Variability	20.4 (r)
ZTF19aascfca	–	AGN Variability	20.7 (g)
ZTF19aascffj	–	AGN Variability	20.0 (g)
ZTF19aatubsj	SN 2019fdr	TDE	17.9 (i)
ZTF19abregmj	AT2020llk	AGN Variability	19.9 (g)
ZTF20aaifyfd	AT2020lll	AGN Variability	19.9 (g)
ZTF20aaifyrs	SN2020awa	SN Ia	17.0 (r)
ZTF20aarbktd	SN2020djn	SN II	18.0 (i)
ZTF20aavnpug	AT2020idu	Dwarf Nova	15.9 (i)
ZTF20aawyens	AT2020lpp	AGN Variability	19.7 (i)
ZTF20aaxcdok	AT2020lpq	Unclassified	20.1 (r)
ZTF20aaxyglx	AT2020llm	AGN Variability	20.3 (g)
ZTF20abaofgz	AT2020lpr	AGN Variability	19.9 (r)
ZTF20abbpkpa	AT 2020lam	SN II	18.8 (g)
ZTF20abcnrcb	–	AGN Variability	19.3 (g)
ZTF20abdnovz	–	Star	21.3 (g)
ZTF20abdnowa	AT2020lln	Artefact	20.7 (g)
ZTF20abdnowp	AT2020llo	Unclassified	21.1 (g)
ZTF20abdnowx	–	AGN Variability	21.3 (g)
ZTF20abdnoxe	–	AGN Variability	20.3 (g)
ZTF20abdnoxm	AT2020llp	Unclassified	20.8 (g)
ZTF20abdnoyu	AT2020lps	Unclassified	21.4 (g)
ZTF20abdnozk	AT2020llq	AGN Variability	20.6 (r)
ZTF20abdnpae	AT2020lpt	Unclassified	20.9 (g)
ZTF20abdnpbp	AT2020llr	AGN Variability	20.7 (r)
ZTF20abdnpbq	AT 2020lpw	AGN Variability	21.0 (r)
ZTF20abdnpbu	AT 2020lpx	Unclassified	21.0 (g)
ZTF20abdnpdo	AT 2020lls	SN Ic	19.0 (r)
ZTF20abdqzjl	–	Star	20.4 (r)
ZTF20abdqzjr	–	AGN Variability	21.1 (g)
ZTF20abdqzkq	AT 2020lpu	Star	20.7 (g)
ZTF20abdqzkr	–	AGN Variability	21.1 (g)
ZTF20abdrnjw	–	Star	21.3 (r)
ZTF20abdrnlg	AT2020lpv	Unclassified	20.9 (r)
ZTF20abdrnmp	–	AGN Variability	21.6 (r)

Table A10. Candidates for IC200530A.

ZTF Name	IAU Name	Classification	Peak Magnitude
ZTF18acvhwtf	AT 2020ncs	AGN Variability	19.7 (r)
ZTF20abgvabi	AT 2020ncr	AGN Variability	20.2 (r)

Table A11. Candidates for IC200620A.

ZTF Name	IAU Name	Classification	Peak Magnitude
ZTF18acccxxf	AT2020tnn	AGN Variability	19.7 (g)
ZTF18adbbnry	AT2020tnn	AGN Variability	19.8 (g)
ZTF20acaapwk	SN2020tno	SN Ia	18.9 (r)
ZTF20acaapwn	–	Unclassified	21.0 (g)
ZTF20acaapwo	AT2020tnp	Unclassified	20.4 (r)
ZTF20acayuno	–	AGN Variability	21.1 (r)

Table A12. Candidates for IC200916A.

ZTF Name	IAU Name	Classification	Peak Magnitude
ZTF18achvmdz	–	AGN Variability	18.9 (i)
ZTF18acwfrle	–	Star	15.4 (g)

Table A13. Candidates for IC200926A.

ZTF Name	IAU Name	Classification	Peak Magnitude
ZTF20aamoxyt	–	AGN Flare	19.8 (g)

Table A14. Candidates for IC200929A.

ZTF Name	IAU Name	Classification	Peak Magnitude
ZTF18abmkdiy	AT2019cvb	AGN Variability	18.7 (i)
ZTF20abfaado	AT2020nbr	Star	19.3 (i)
ZTF20acinqzo	–	AGN Variability	19.6 (i)
ZTF20acmxnpa	AT2020ybb	Unclassified	20.6 (g)

Table A15. Candidates for IC201021A.

ZTF Name	IAU Name	Classification	Peak Magnitude
ZTF17aadmvpm	–	Artefact	16.1 (g)
ZTF18abxrpgu	AT2021ury	AGN Flare	18.8 (r)
ZTF18achpvrl	–	AGN Variability	19.1 (r)
ZTF19aaagxcv	–	AGN Variability	18.4 (g)
ZTF20aceidvg	–	AGN Variability	19.7 (g)
ZTF20acmnnwf	–	AGN Variability	19.9 (r)
ZTF20acuqdeu	AT2020aehs	Unclassified	19.8 (g)
ZTF20acxbkpz	–	Unclassified	20.5 (r)

Table A16. Candidates for IC201130A.

ZTF Name	IAU Name	Classification	Peak Magnitude
ZTF18abwhosy	–	AGN Variability	19.3 (r)
ZTF20abvxjup	–	AGN Variability	20.0 (g)
ZTF20acycunv	SN2020addp	SN IIP	19.4 (r)

Table A17. Candidates for IC201209A.

ZTF Name	IAU Name	Classification	Peak Magnitude
ZTF19aaapmca	–	AGN Variability	18.6 (r)
ZTF19aailrrn	–	AGN Variability	20.0 (g)
ZTF19aasfvho	–	AGN Variability	19.4 (g)
ZTF19aasfvqm	–	AGN Flare	18.2 (r)
ZTF20aadynqa	–	AGN Variability	20.1 (g)
ZTF20aajcpde	–	AGN Variability	19.5 (g)
ZTF21aafmkun	–	AGN Variability	19.4 (r)
ZTF21aajxjmv	–	Star	21.3 (r)
ZTF21aajxjmy	–	Star	21.1 (g)
ZTF21aajxjnb	–	AGN Variability	22.1 (g)
ZTF21aajxjnc	–	AGN Variability	21.7 (g)
ZTF21aajxjrn	–	AGN Variability	20.1 (r)
ZTF21aajxjrv	AT2021clu	Unclassified	20.9 (r)
ZTF21aajxjry	AT2021clv	Unclassified	21.5 (r)
ZTF21aajxjsa	–	AGN Variability	21.7 (r)
ZTF21aajxkls	–	AGN Variability	21.1 (g)
ZTF21aakiqpj	–	Star	22.1 (g)

Table A18. Candidates for IC210210A.

ZTF Name	IAU Name	Classification	Peak Magnitude
ZTF19aadzayi	–	Star	15.0 (r)
ZTF19aawqcum	–	AGN Variability	19.1 (g)
ZTF20abhfiyd	–	Star	19.6 (g)
ZTF20acinvxv	–	Unclassified	21.0 (r)
ZTF20acinwlt	–	AGN Variability	21.0 (r)
ZTF21aaiuekm	–	Star	19.5 (g)

Table A19. Candidates for IC210510A.

ZTF Name	IAU Name	Classification	Peak Magnitude
ZTF18abteipt	AT2019gnu	AGN Variability	17.1 (r)
ZTF21abecljv	AT2021osi	AGN Variability	19.8 (i)
ZTF21abllruf	–	Artefact	17.5 (i)

Table A20. Candidates for IC210629A.

ZTF Name	IAU Name	Classification	Peak Magnitude
ZTF20abjezpo	–	Star	19.7 (r)
ZTF21absmcwm	–	AGN Variability	20.8 (g)

Table A21. Candidates for IC210811A.